Physical and Chemical Characterization of Chinese Maize Stalk Leaf Ash: Calcining Temperature and Aqueous Solution

Guorui Feng,[a,c] Tingye Qi,[a,b,c,*] Zehua Wang,[a,c] Jinwen Bai,[a,c] and Zhen Li [a,c]

This study focused on the physical and chemical characterization of Chinese maize stalk leaf ash (MSLA) calcined at 500, 700, and 850 ℃ and MSLA residual leaching in aqueous solutions. The grain size distribution, chemical composition, and microstructure of MSLA were investigated using a laser Mastersizer, X-ray fluorescence, and scanning electron microscopy. The ash samples obtained before and after dissolving were analyzed using X-ray powder diffraction and X-ray photoelectron spectroscopy to identify the present minerals and observe the 2p atomic orbit of surface silicon and aluminum (Si 2p and Al 2p) transformation behaviors. The zeta potential and pH values of hybrid solutions were tested for various dissolving times. Silica was the predominant component observed in the MSLA. As dissolving time increased, the pH value gradually decreased, and the zeta potentials first slightly decreased and then remarkably increased. Quartz was identified in the MSLA. Another polymorphous crystalline form of silica, cristobalite, only appeared in the 850 °C sample. The binding energies of Si 2p and Al 2p shifted, which transformed the XPS peaks after the thermal and aqueous solution treatment of MSLA. These findings can be utilized to study the application potential of MSLA in cementing systems.

Keywords: Maize stalk leaf ash; Calcination temperature; Aqueous solution; Silica

*Contact information: a: College of Mining Technology, Taiyuan University of Technology, Taiyuan, China; b: State Key Laboratory of Coal Resources and Safe Mining, China University of Mining and Technology, Xuzhou, China; c: Shanxi Province Research Center of Green Mining Engineering Technology, Taiyuan, China; *Corresponding author: qty198402@163.com*

INTRODUCTION

Biomass as fuel is mainly used to generate electricity and provide heat. In 2020, the projected biomass output produced for direct combustion power generation will be approximately 1.4×10^7 t. China is the most prominent crop-producing region of the world and produces a large amount of biomass waste every year, especially maize waste. The gross weight of maize straw is approximately 2.4 billion t, which accounts for 24.2% of the total crop output in China (Vassilev *et al.* 2013a; Zhang *et al.* 2016). Moreover, the maize stalk is a primary source of fuel for biomass power plants. The elements in maize stalk ash are primarily Si, K, Ca, and Mg (Xiong *et al.* 2010). The disposal and use of the large maize ash waste from a power plant must be considered. Biomass ash has been reused in many ways, such as for removing methylene blue from water (Liu *et al.* 2018), producing geopolymers due to the silica content (Zarina *et al.* 2013), and applications in construction.

Biomass ash has been widely used as the raw material to improve the rheological properties of grout and the mechanics of the solidification bodies for cement-based

materials. Moreover, the pozzolanic activity and negative surface charge of biomass ash have been considered (Givi *et al.* 2010; Maldonado-Bandala *et al.* 2011). Biomass ash from thermal treatment contains SiO_2, Al_2O_3, and Fe_2O_3, suggesting the possibility of exhibiting pozzolanic properties (Rajamma *et al.* 2009). Active silica and alumina are very useful materials that react with calcium hydroxide to produce the C-S-H, which contributes to improving the strength of cement-based materials (Biricik *et al.* 1999). Calcination can impart pozzolanic activity to biomass ashes, such as palm oil clinker powder, wheat straw ash, sugar cane bagasse ash, and sugar cane straw ash (Cociña *et al.* 2013; Moraes *et al.* 2015; Karim *et al.* 2016).

The combustion temperature can influence the composition, microstructure, and pozzolanic properties of different kinds of biomass ash. Rice husk calcined at 500, 600, 700, and 800 ℃ was tested for its compressive strength and analyzed using X-ray powder diffraction (XRD), and it was concluded that the optimum combustion temperature for obtaining highly reactive rice husk ash (RHA) is 600 ℃ (Xu *et al.* 2012). Sugar cane straw ash (SCSA) with 20% and 30% clay content burned at 800 and 1000 ℃ and then reacted with lime showed that SCSA has good pozzolanic activity, comparable to that of rice husk ash (Cociña *et al.* 2003). The consistent results reported by Morales *et al.* (2009) showed that sugar cane waste ash calcined at 800 and 1000 ℃ have properties indicative of high pozzolanic activity. It is very interesting that identical species of biomass ash from different production areas require different calcination temperatures to yield high pozzolanic activity. Brazilian bamboo leaf ash calcined at 600 ℃ had a very high pozzolanic activity (Frías *et al.* 2012). However, Cuban bamboo leaf ash calcined at 500, 600, and 700 ℃ was evaluated for pozzolanic activity by using a conductometric method, and it was found that Cuban bamboo leaf ash calcined at 500 ℃ showed the highest pozzolanic activity (Cociña *et al.* 2018).

When the ash deformation temperatures of biomass ash were investigated, it was found that calcination temperatures ≥ 550 ℃ completely removed the organic matter from rice straw. Further, the ashes underwent significant sintering when calcined at 650 ℃ due to the presence of potassium chloride (Roselló *et al.* 2017). In addition, the ash deformation temperatures of red pine and straw were over 1100 ℃ (Fang and Jia 2012).

The minerals and phases containing Si and Al elements are transformed during the combustion of biomass ash. Due to the presence of totally crystalline silica in the original rice husk ash prepared at 800 °C, a leaching procedure, low calcination temperature, and short calcination time were proposed to prepare more active amorphous silica from rice husk (Shen *et al.* 2011). The porosity of lemon grass ash and the crystallinity of the silica in the lemon grass ash increased as the calcination temperature was increased from 0 to 700 ℃ (Firdaus *et al.* 2016). Bamboo leaf fired in an open atmosphere and then heated at 600 ℃ for 2 h in a furnace is an amorphous material containing amorphous silica (Dwivedia *et al.* 2006). In addition, based on Vassilev *et al.* (2013b), fluxing and refractory behaviors of different modes of elements occur during the combustion of biomass according to the melting point (MP) of the minerals and phases containing Al elements. Elemental Al, K-Al sulphate, K-aluminosilicate, and albite appeared at 660, 690 to 800, 695, and 1118 ℃ calcination temperatures, respectively. The K feldspar, microcline, orthoclase, and sanidine appeared at 1170 ℃, whereas biotite, chlorite, and muscovite appeared at 1200 ℃.

Above all, the factors that influence the physical and chemical properties of the biomass ash were the calcination temperature, components of the biomass, production location, and biomass species. However, the evolution of the physical and chemical

properties for maize stalk, and in particular maize stalk leaf ash (MSLA) in China, with increasing calcination temperature has been rarely reported. The change of the characteristics after thermal and aqueous solution treatment (water is the primary raw material in cement-based materials) must be investigated. It is essential to develop environmentally friendly and inexpensive management of maize straw ash.

In this study, the composition and microstructure of maize stalk leaf ash calcined at 500, 700, and 850 ℃ were investigated. The pH values and zeta potentials of MSLA mixed in deionized water for 0 to 2 h were measured. The mineralogy, Si 2p, and Al 2p chemical bonds of the calcined MSLA, and water-leaching residue were investigated. This knowledge is essential for understanding the effect of calcination temperature on the characteristics of MSLA and the water-leaching properties of MSLA. These conclusions will be useful for assessing the possibility of using MSLA in cementing systems.

EXPERIMENTAL

Materials

The maize stalk leaf samples from Shanxi province China were obtained with the stems removed. The stalk leaves were washed using tap water to remove impurities, dried at 105 ℃ for 24 h in a circulating oven, and then were crushed to a 1-cm grain size. The crushed leaves were placed into a muffle furnace to calcine for 3 h at 500, 700, or 850 ℃. Then, the cooled MSLA was milled and filtered using a 0.074-mm membrane filter, and the samples were characterized using a Laser particle size analyzer, X-ray photoelectron spectroscopy (XPS), scanning electron microscopy (SEM), and X-ray powder diffraction (XRD). The filtered solid samples from the three calcination temperatures were dissolved in deionized water at a liquid-to-solid (L/S) ratio of 2/15 L/g. The pH values of the solutions were tested at 15 min intervals for 2 h, and the zeta potentials were measured after 30, 60, and 90 min. The residues after leaching for 30 and 120 min were oven-dried at 80 ℃. The XRD and X-ray fluorescence (XRF) analyses of the dried residue were performed. Figure 1 shows the preparation process of the straw stalk leaf ash samples.

Fig. 1. Process of preparing straw stalk leaf ash samples

Methods

The grain size distribution (GSD) of MSLA is an important property, because it can affect the resultant paste consistency, chemical reactivity, and the overall hydromechanical properties. The GSD curves of the MSLA samples were determined using a Malvern Laser Mastersizer S 2000 (Malvern Instruments Inc., Worcestershire, UK), which is capable of measuring particles between 0.05 and 880 μm with an accuracy of ± 1%.

An XPS analysis was performed using an Axis Ultra DLD instrument (Kratos, Manchester, UK) for surface characterization. The powder samples were heated for approximately 2 h at 80 °C in air to reduce the amount of adsorbed water. Immediately after removing them from the oven, the samples were fixed on adhesive tape and introduced into the vacuum system. Photoelectron emission was excited *via* a monochromatic Al Kα line with photon energy of 1486.67 eV.

The microstructure analysis of MSLA samples was performed using a JEOL JSM 6390 LV (JEOL Ltd., Tokyo, Japan) electron microscope at 25 kV. The samples were previously Au coated (SKY Technology Development Corp., Shenyang, China) to avoid charging problems.

The MSLA and MSLA residuals were characterized by X-ray powder diffractometry using an Ultima IV Rigaku diffractometer (Rigaku Corp., Tokyo, Japan) equipped with Cu Kα1, 2 (λ = 1.54178 Å) radiation with a generator voltage of 40.0 kV and a current of 40.0 mA. The 2θ range of 5° to 90° was used for all powders in continuous scan mode with a scanning step of 0.02° at a rate of 10°/min.

The main chemical composition of MSLA (in the form of oxides) was determined by XRF (ZSX Primus II; Rigaku Corp., Tokyo, Japan). The samples used for XRF testing were heated at 550 °C for 2 h, according to GB/T 28731 (2012). The softening temperatures (ST) were measured according to GB/T 30726 (2014).

The zeta potentials in the aqueous solutions of MSLA were characterized using a microscopic electrophoresis apparatus (JS94H; Powereach Corp., Shanghai, China) with an Ag electrode. The measurement parameters were: particle size range of 0.5 to 20 μm, input pH range of 1.6 to 13.0, step length of 0.1, and switching time of 700 ms. The pH values of the solutions were measured using a LEICI PHSJ-3 (INESA Scientific Instrument Co., Ltd., Shanghai, China) pH meter, and the criterion pH value was adjusted before each measurement.

RESULTS AND DISCUSSION

Particle Size Distribution

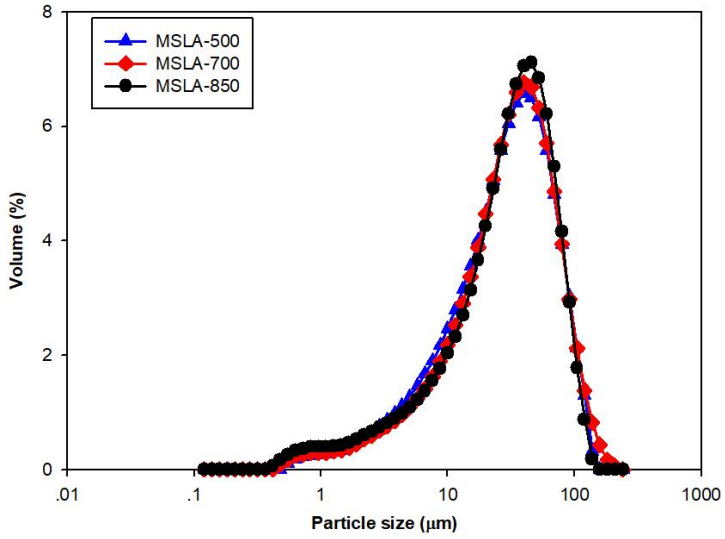

Fig. 2. Grain size distribution of MSLA calcined at 500, 700, and 850 °C

According to the GSD curves of the samples (0.074 mm) (Fig. 2) and Table 1, the specific surface areas slightly increased with increasing calcination temperature. The particle sizes of MSLA with different calcination temperatures were close to a continuous gradation.

Chemical Composition

As shown in Table 1, the loss on ignition increased with increasing temperature. The chemical compositions of the maize stalk ashes, shown in Table 1, varied depending on the combustion temperature. Silica, potassium oxide, magnesium oxide, and lime compounds were predominantly observed in the samples. The abundance of K in MSLA together with the high Si content favors the formation of alkali-rich silicates and thus decreases the ash melting temperature (Zhu *et al.* 2018).

Table 1. Chemical Composition of Maize Stalk Leaf Calcined at 500, 700, and 850 °C

	MSLA-500	MSLA-700	MSLA-850
SiO_2 (%)	67.02	72.86	73.53
Al_2O_3 (%)	2.15	2.09	2.64
Fe_2O_3 (%)	1.01	1.02	1.27
CaO (%)	6.78	7.72	7.99
MgO (%)	3.68	4.29	4.29
SO_3 (%)	2.42	1.96	2.25
TiO_2 (%)	0.13	0.12	0.16
K_2O (%)	5.24	4.91	3.80
Na_2O (%)	0.40	0.50	0.57
P_2O_5 (%)	0.94	0.97	1.08
Cl (%)	0.39	0.25	-----
CuO (%)	0.23	0.21	0.10
SUM (%)	89.77	96.44	97.58
LOI (%)	89.41	90.67	91.48
Specific Surface Area (m^2/g)	0.534	0.550	0.633

Meanwhile, the contents of refractory species Mg, Ca, Fe, Al, Si, S, and P were nearly constant or slightly increased with temperature. This increase was attributed to the increase of the relative content of these elements with the release of volatile species. The increase of Mg, Ca, P, and S contents in the ash implies that high melting temperature substances were formed (Bostrom *et al.* 2011). The chemical composition of MSLA is similar to that of sugarcane biomass ash (Katare and Madurwar 2017) and rice straw ash (Wang *et al.* 2013). The SiO_2, Al_2O_3, and Fe_3O_4 are the main active pozzolanic substances. The Si content was remarkably higher than the Al and Fe contents. Thus, Si was the major pozzolanic substance in the cement-based-MSLA system.

pH Value

When the calcined MSLA samples were dissolved in deionized water within 0 to 120 min, the order of pH values was MSLA-500 > MSLA-700 > MSLA-850 at all dissolving times (Fig. 3). This was due to the higher concentration of OH^- in the MSLA-500 aqueous solution. The aqueous solutions of the MSLA samples were alkaline due to the high K_2O and CaO contents of MSLA (Font *et al.* 2017). The MSLA could be used as an alkali source in alkali-activated materials.

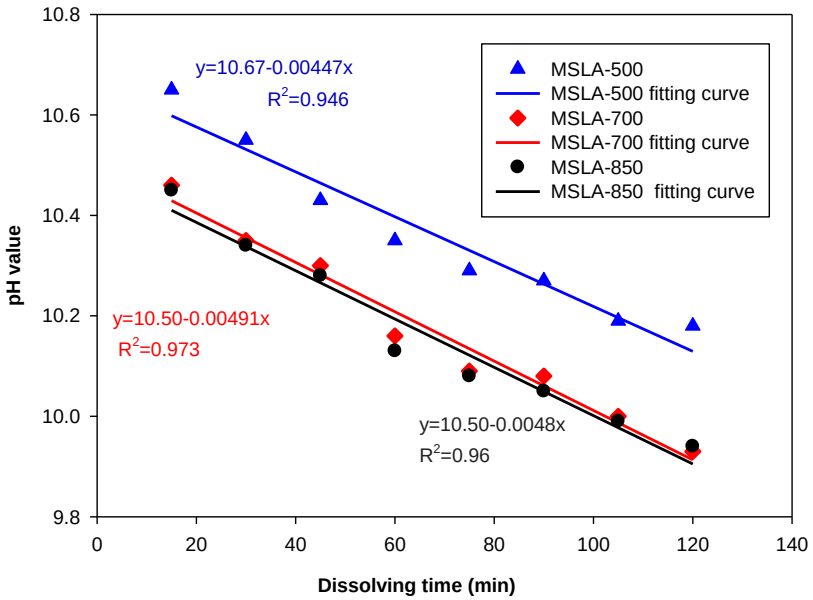

Fig. 3. The relationship between pH value and dissolving time of MSLA-500, MSLA-700, and MSLA-850 mixing in the aqueous solution

The pH value decreased with increasing dissolving time, due to the consumption of OH^- ions that participate in the chemical reactions producing more –OH minerals (seen from the XRD in the MSLA residuals). The pH curves were fit using linear regression and yielded equations with negative slopes.

Amorphous SiO_2 and Al_2O_3 might have been responsible for the decreasing pH of the aqueous solutions. The silicate precursors were formed *in situ* through dissolution of amorphous silica particles by the alkaline solutions (Simonsen *et al.* 2009a). The dissolution of the amorphous silica in alkaline conditions can produce H_4SiO_4, $H_3SiO_4^-$, and $H_2SiO_4^{2-}$. These reactions suggest that H_2O and OH^- are consumed during the dissolution process, resulting in a decrease in pH that also was observed experimentally (Simonsen *et al.* 2009b). In contrast, the amorphous Al_2O_3 reacted with OH^- to form amorphous $Al(OH)_3$ in the alkali aqueous solution, which also leads to the decrease in the pH values of the aqueous solutions (Dijkstra *et al.* 2006).

Zeta Potential

To see the role of surface charge on repulsion, the zeta potential of the MSLA was calculated and found to have a negative value (Table 2). This result indicated that the surfaces of the MSLA particles had moderate negative charges. The electronegative surface of MSLA might have been due to the presence of minerals and unburnt biomolecules in the MSLA.

Table 2. Zeta Potential (mV) of MSLA Calcined at 500, 700, and 850 °C Dissolving in Aqueous Solution for 30, 60, and 90 min

Calcination Temperature (°C)	Dissolving Time (min) / Zeta Potential (eV)		
	30	60	90
500	-1.98	-1.13	-5.23
700	-2.26	-2.24	-11.58
850	-2.27	-2.25	-19.17

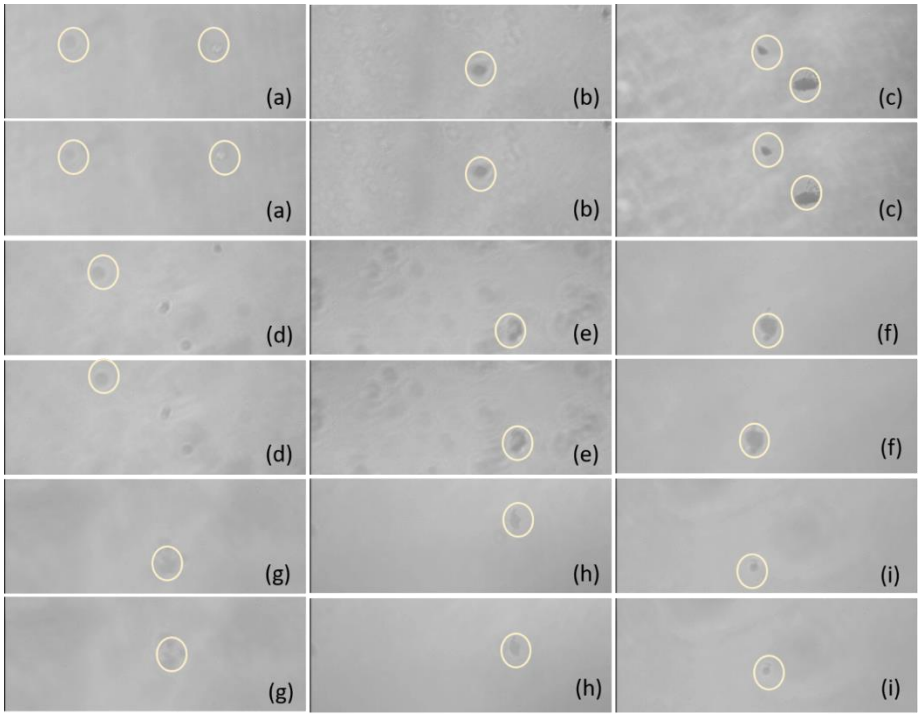

Fig. 5. The movement of MSLA-500 particles in an electric field after (a) 30 min, (b) 60 min, and (c) 90 min of dissolving time. The movement of MSLA-700 particles in an electric field after (d) 30 min, (e) 60 min, and (f) 90 min of dissolving time. The movement of MSLA-850 particles in an electric field after (g) 30 min, (h) 60 min, and (i) 90 min of dissolving time. The two pictures for each letter to show the MSLA particle movement for the two opposite direction currents of the electric field in the aqueous solution.

An electronegative surface of MSLA can be more beneficial for repulsion of the anions of cement. It was found that the zeta potentials first slightly decreased and then sharply increased with increased dissolving time, changing into a ‘‘V’’ shape. Moreover, the zeta potential of the 850 ℃ sample showed a higher value and higher rise rate than those of the samples calcined at the other temperatures. When the alkali metal ions dissolved in the aqueous solutions, alkali metal ions (*e.g.*, potassium, sodium, and calcium) neutralized the negative charges and reacted with the OH^- at the surface of the MSLA producing new minerals that wrap the particles, which led to compression of the electric double layer due to electrostatic interactions. This may explain the decline of the zeta potential in the interval of 30 to 60 min. As the dissolving time increased, the surfaces of the particles constantly absorbed OH^- from the aqueous solution, which added to the negative charge. This may explain the ascent of the zeta potential in the interval of 60 to 90 min (Moghal and Sivapullaiah 2012). Figure 5 shows the MSLA particles with different calcination temperatures and dissolving times moving in the electric field. Larger values of the zeta potential led to a larger relative distance traversed by the MSLA particles in the electric field.

Therefore, this suggests that adding the MSLA-850 in the cement system improved the flowability of the slurry for the cemented paste backfill (CPB) or the cemented coal gangue backfill (CGB) due to the repulsion of the MSLA particles by the identically charged surfaces of the cement particles, preventing flocculation (Givi *et al.* 2010).

SEM

As can be seen in Fig. 6a, the morphology of the MSLA after calcination at 500 ℃ showed a tubular porous aggregate shape. This characteristic was due to the removal of the hemicellulose, cellulose, and lignin after calcination at 500 ℃.

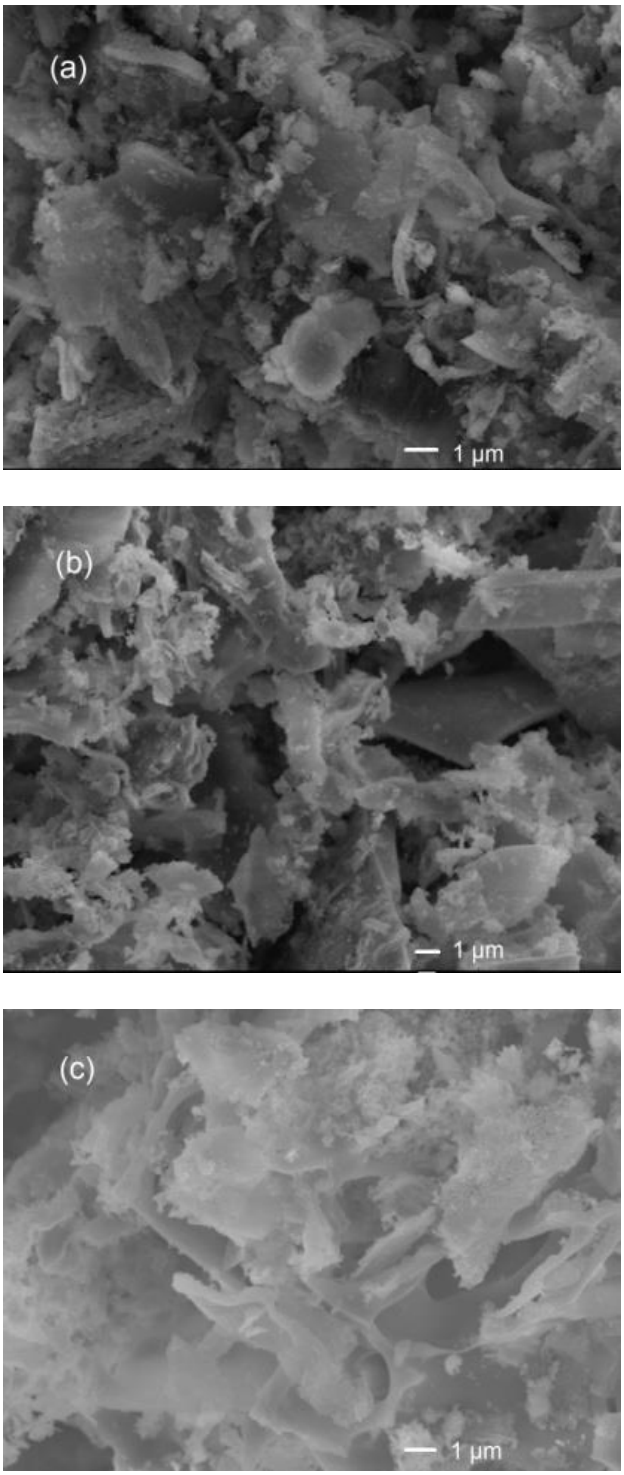

Fig. 6. SEM images of MSLA with different calcination temperatures: (a) 500 °C, (b) 700 °C, and 850 °C

The irregularly shaped particles were distributed on the surface of MSLA-700 (shown in Fig. 6b). The SEM images obtained confirm that particle aggregation occurred when the samples were thermally treated. Increasing the treatment temperature promoted the emergence of a more intact structure. Compared to MSLA thermally treated at temperatures below 700 ℃, larger numbers of agglomerated particles and polyporous structures were observed for the MSLA treated at 850 ℃ (Fig. 6c).

XRD

Silica has three main polymorphous crystalline forms, quartz, tridymite, and cristobalite, all with relatively complex structures and atoms that are not closely packed (Callister and Rethwisch 2010).

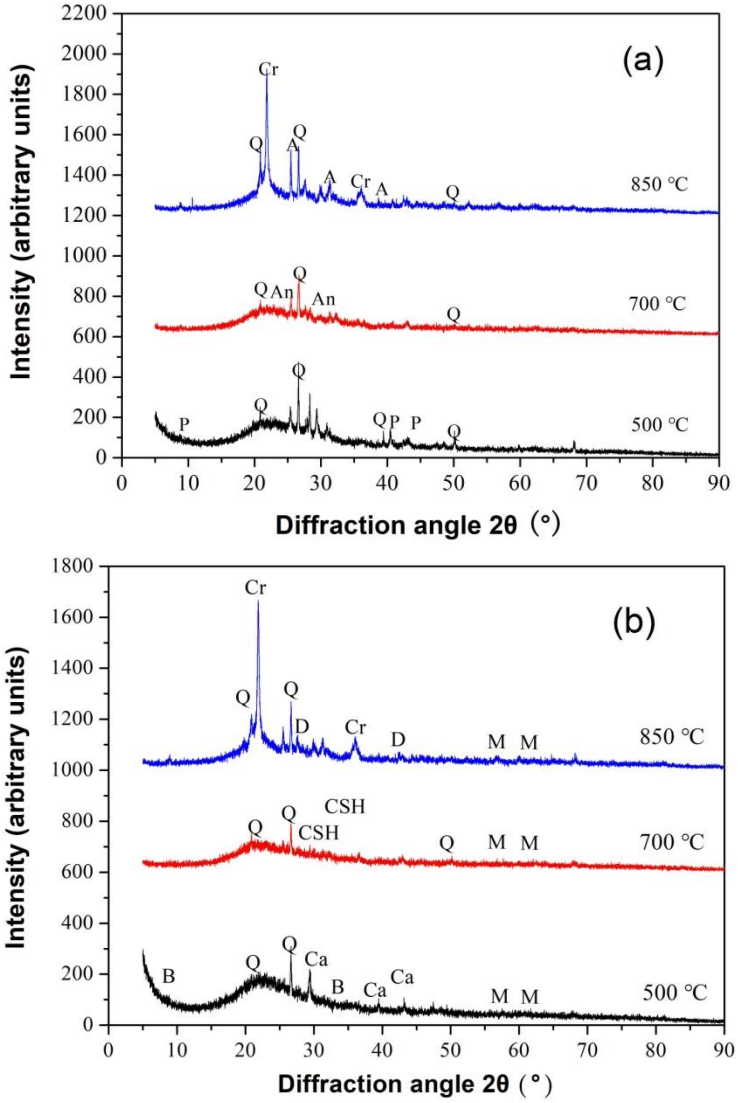

Fig. 7. XRD patterns for MSLA-500, MSLA-700, and MSLA-850 for (a) no dissolving and (b) dissolving for 120 min; Key: Q = Quartz SiO_2; An = Anorthite $Ca(Al_2Si_2O_8)$; A = Anhydrite $CaSO_4$; Cr = Cristobalite SiO_2; Ca = Calcium Carbonate $CaCO_3$; B = Biotite $KMg_3AlSi_3O_{10}OHF$; M = Muscovite $KAl_{2.20}(Si_3Al)_{0.975}O_{10}((OH)_{1.72}O_{0.28})$; CSH= Calcium Silicate Hydrate $Ca_{1.5}SiO_{3.5} \cdot XH_2O$; and D = Diopside $CaMgSi_2O_6$

The diffractogram peaks obtained for the thermally treated maize stalk leaves show that the ash type has the quartz silica form (Fig. 7a), whose peak is marked in the diffractograms for the MSLA samples. The peak of the other silica form, cristobalite, was observed only in the 850 ℃ sample, which is much less than the theoretical temperature of thermal transformations of pure silica into cristobalite (Pagliari *et al.* 2013). The reason is that MSLA contains, in addition to SiO_2, compounds with high alkali metal levels and contaminants that may affect the melting point and crystallization (Soltani *et al.* 2015). Furthermore, the amorphous silica in the MSLA was inclined to transform into cristobalite rather than tridymite, mainly due to the existence of crystal nuclei of cristobalite formed from the opal-cristobalite phase transition (Zheng *et al.* 2018). A previous study also showed that the silica phase transformation in RHA begins at 600 and 800 ℃, and the cristobalite phase begins at 800 ℃ (Kapur 1985; Fernandes *et al.* 2017). However, it should be mentioned that a portion of the ash components was probably present in an amorphous phase, which could not be identified by XRD analysis.

In addition, muscovite was found in the MSLA residual (Fig. 7b), because alkali hydroxides mostly dominated at high pH values in the aqueous solution (from pH test results). The surface of MSLA was negatively charged (from the zeta potential results); metals are adsorbed in the MSLA with a strong tendency to form chemical bonds between the metal groups and the oxide surface (Liu *et al.* 2018).

XPS

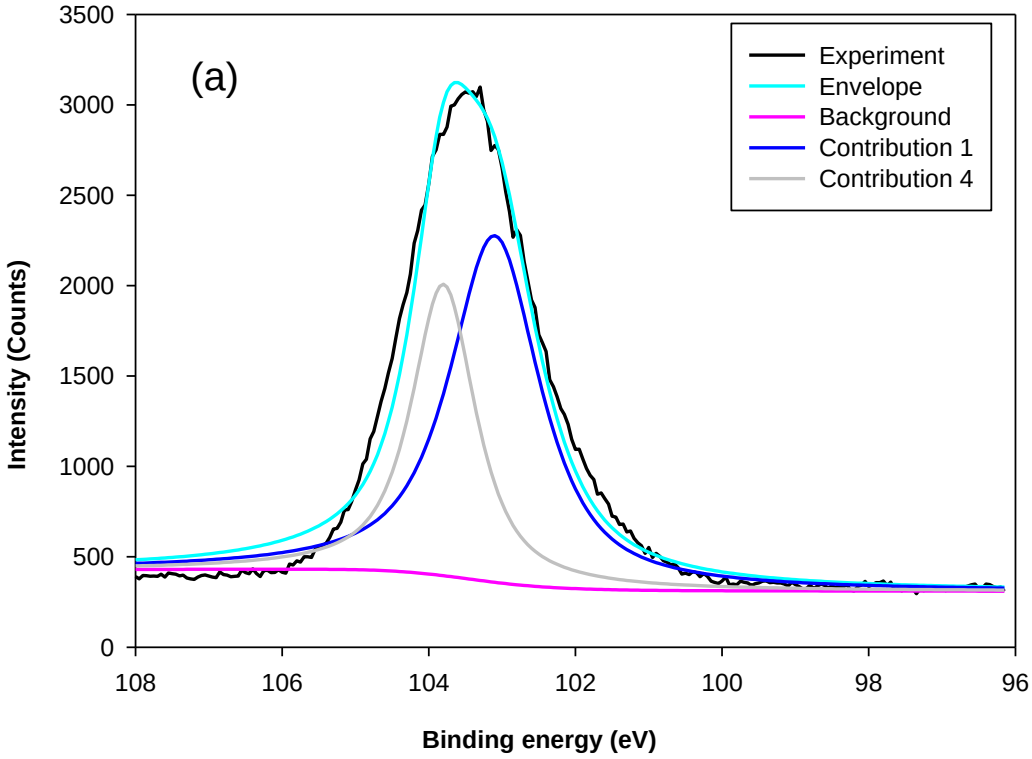

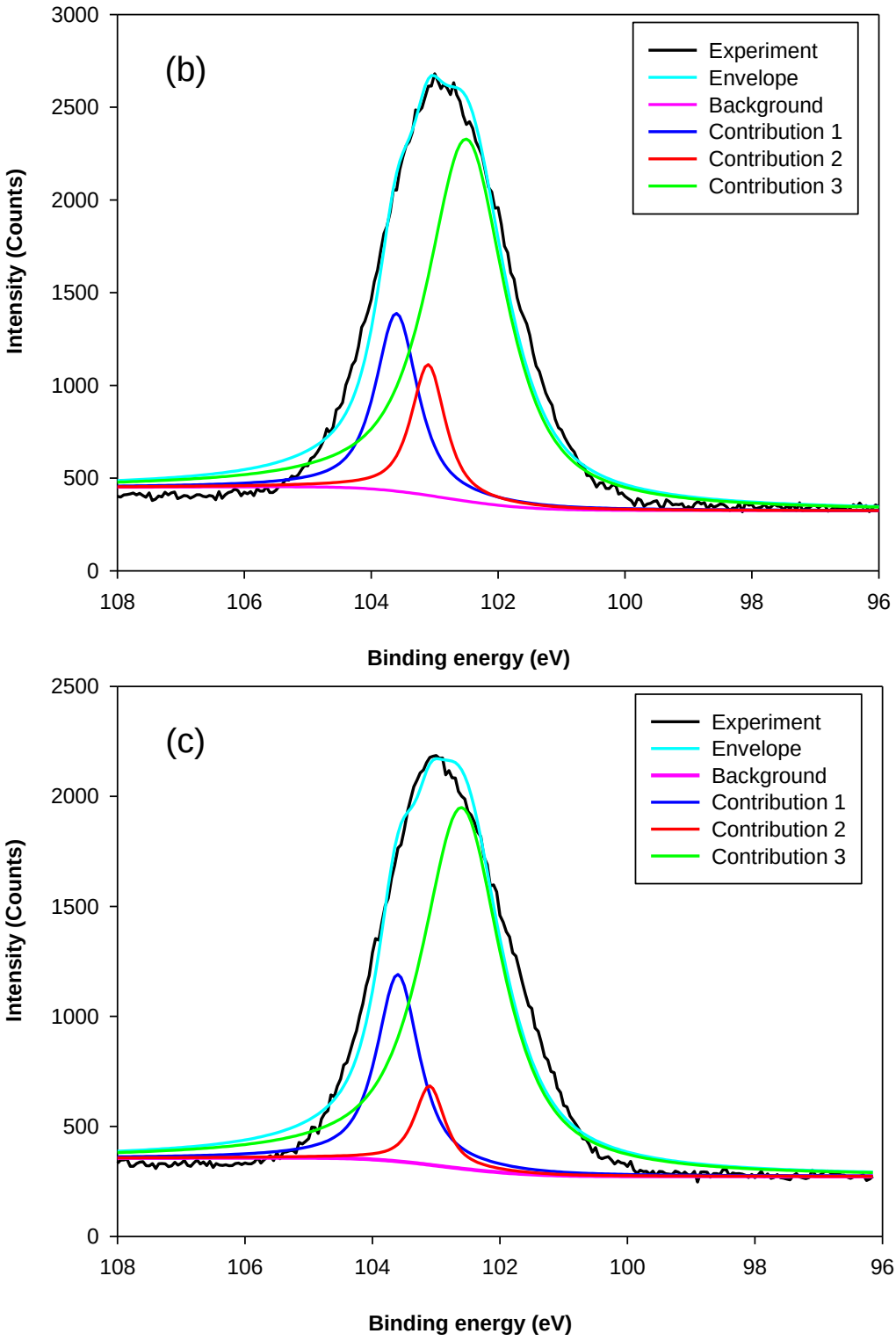

Fig. 8. The typical Si 2p XPS survey spectra for MSLA at (a) 500, (b) 700, and (c) 850 °C

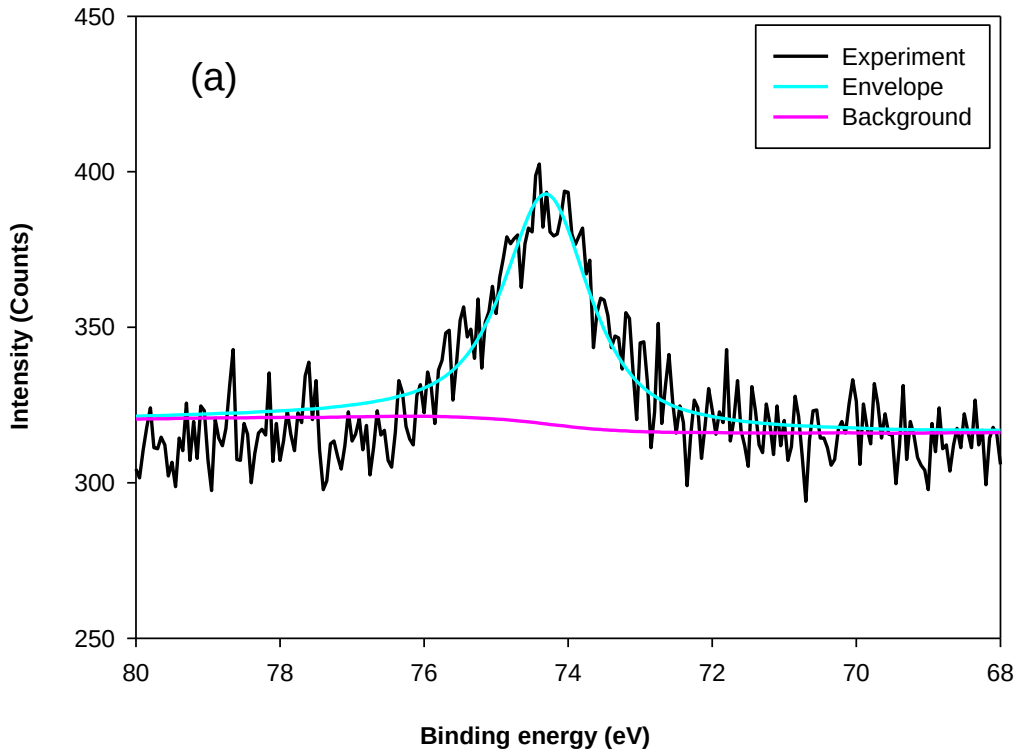
(a)
Experiment
Envelope
Background
Intensity (Counts)
450
400
350
300
250
80
78
76
74
72
70
68
Binding energy (eV)

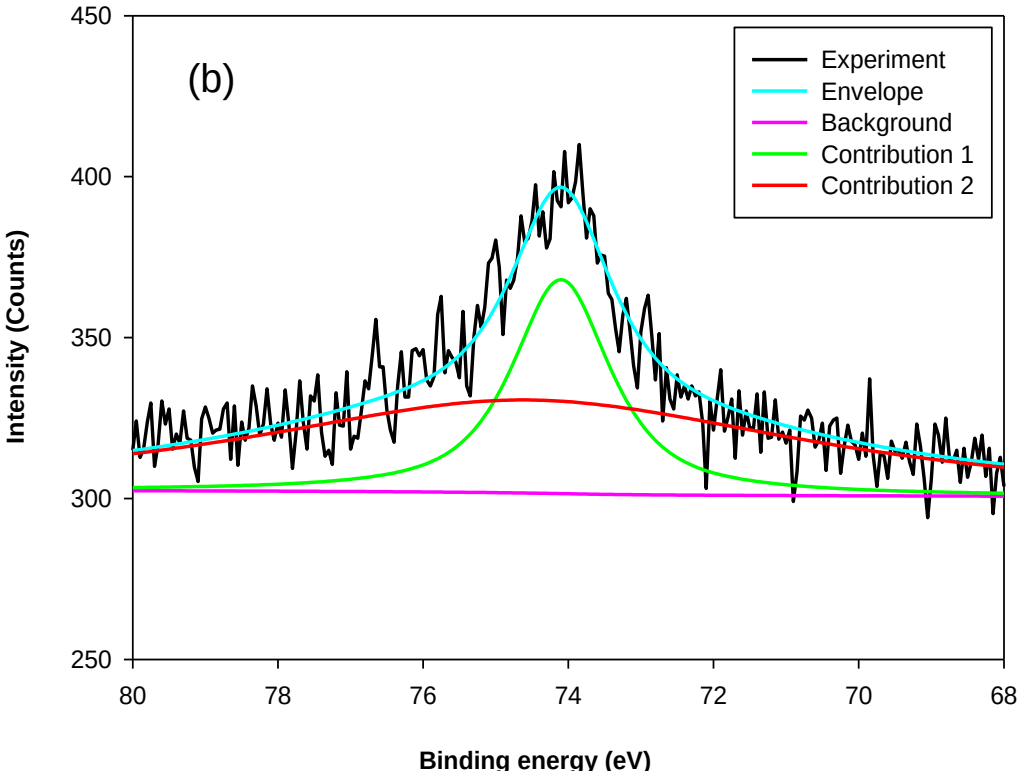
(b)
Experiment
Envelope
Background
Contribution 1
Contribution 2
Intensity (Counts)
450
400
350
300
250
80
78
76
74
72
70
68
Binding energy (eV)

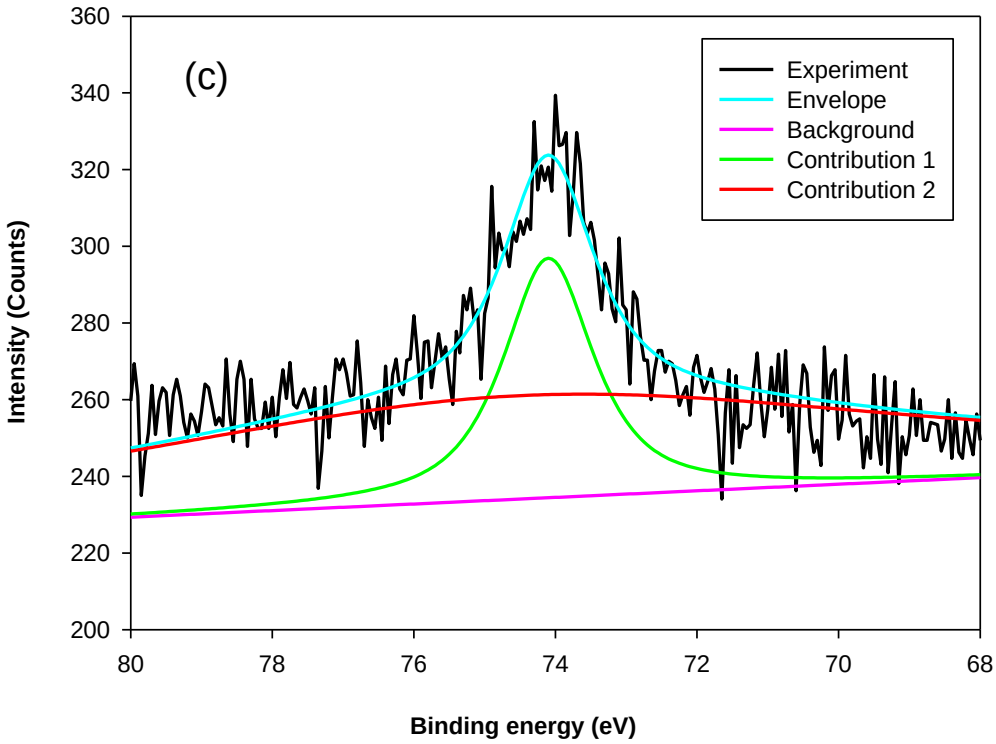

Fig. 9. The typical Al 2p XPS survey spectra for MSLA at (a) 500, (b) 700, and (c) 850 °C

Table 3. Fitting Results of the Si 2p and Al 2p Lines Taken From MSLA-500, MSLA-700, and MSLA-850

Sample	Si 2p $_{3/2}$ (eV/ %)				Al 2p $_{3/2}$ (eV/ %)	
	Contrib. 1	Contrib. 2	Contrib. 3	Contrib. 4	Contrib. 1	Contrib. 2
MSA-500	----	103.1/ 62.8%	----	103.8/ 37.2%	74.3	----
MSA-700	103.6/ 18.6%	103.1/ 11.1%	102.6/ 70.3%	----	74.1/ 29.0%	74.5/ 71.0%
MSA-850	103.6/ 20.3%	103.1/ 6.1%	102.6/ 73.6%	----	74.1/ 79.3%	74.5/ 20.7%

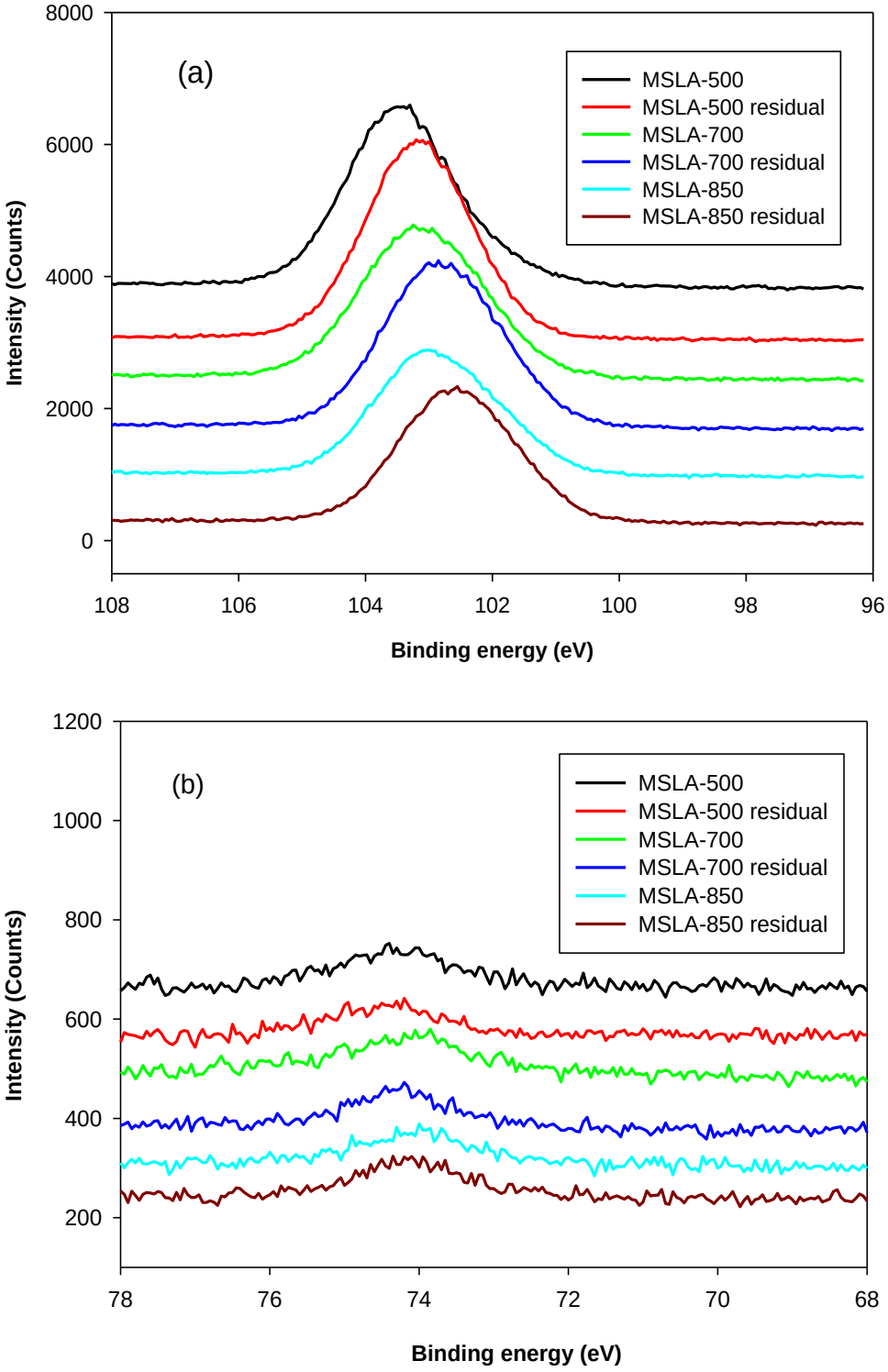

Fig. 10. (a) Si 2p and (b) Al 2p line shifts of the MSLA calcined at 500, 700, and 850 °C after mixing in aqueous solution for 120 min

The instrument used for XPS is widely applicable for probing the surface chemical composition and atomic structure of biomass ash.The fit results for Si 2p and Al 2p lines, shown in Table 3, give detailed insight into the MSLA and residual structure. Figures 8

and 9 show the fit curves of the Si 2p and Al 2p lines obtained for MSLA with different calcination temperatures, respectively. The Si 2p lines in MSLA-500 were resolved into two contributions. It should be noted that the position of this line depended on the number of sialate bonds. For instance, for pure siloxo Si-O-Si bonds, the position of Si $2p_{3/2}$ was as high as 103.8 eV (Paparazzo *et al.* 1992). The second contribution of the Si $2p_{3/2}$ line was situated at approximately 103.1 eV, corresponding to quartz. However, the position of the Si 2p line of MSLA-700 and MSLA-850 located at 103.8 eV disappeared, and at least three contributions were expected: one at approximately 103.6 eV attributed to Si-O-Si bonds, one at approximately 103.1 eV attributed to quartz (and cristobalite in MSLA-850), and one related to Si-OX bonds, which was as high as 102.6 eV (Kljajević *et al.* 2017). As the calcination temperature increased to 850 ℃, the relative content of Si-OX bonds increased. It can be concluded that annealing at 700 ℃ resulted in the destruction of some Si-O-Si groups and the formation of another silicon compound; a possible candidate is anorthite, which corresponds to the position of peak 3. Additionally, anorthite was detected by XRD in MSLA-700.

When the MSLA dissolved in the aqueous solution, the binding energies of Si 2p shifted to a lower position (shown in Fig. 10a) because of the formation of surface site $> SiO^-$ (deprotonated surface sites) in the alkaline solutions. The higher amount of silicon released from cristobalite compared to that from quartz was due to the crucial effect of structural defects associated with oxygen vacancies with positive charges.

Under alkaline conditions, the surface silanols interacted with OH^- to form neutral, positive, or negative surface species *via* deprotonation calculated by Eq. 1 (Zhu *et al.* 2017),

$$> SiOH + OH^- = > SiO^- + H_2O \quad (1)$$

where $> SiOH$ denotes the deprotonated surface sites. The characteristics of the surface sites could remarkably affect the solubility and reaction mechanisms of the silica minerals (Gratz and Bird 1993).

For the Al 2p line of MSLA-500, the only peak (at approximately 74.3 eV) was related to octahedral-coordinated bonds fit to Al $2p_{3/2}$. For MSLA-700, the Al $2p_{3/2}$ was resolved into two contributions. The first peak was related to an octahedral-coordinated bond, whose position shifted towards lower binding energies by roughly 0.2 eV, corresponding to the Al $2p_{3/2}$ lines of MSLA-700. The second peak was related to tetrahedral-coordinated bonds, situated at approximately 74.5 eV. However, the relative content of Al $2p_{3/2}$ for the octahedral-coordinated bond sharply increased as the calcination temperature increased. The electronic environment with the octahedral-coordinated Al ion was more polarizable than that with the tetrahedral-coordinated Al ion. When the MSLA was dissolved in an aqueous solution, the binding energy of the Al 2p peak remarkably increased (Fig. 10b). This is an Al mineral structural dissimilarity between the MSLA and MSLA residual, caused by a change in the electronic and chemical environment (Black *et al.* 2003; Li *et al.* 2008). The Si 2p and Al 2p bond transformation behavior implied that the MSLA could react with lime to produce C-S-H.

CONCLUSIONS

1. The particle size of maize stalk leaf ash (MSLA) was close to a continuous gradation. Silica was the predominant component observed in MSLA. The order of the pH values

was MSLA-500 > MSLA-700 > MSLA-850 for all dissolving times. The pH values gradually decreased with increasing dissolving time, and there was a linear relationship between pH and dissolving time.

2. The zeta potentials first slightly decreased and then remarkably increased with increasing dissolving time, changing into a ‘‘V’’ shape. The zeta potential of the 850 ℃ sample had the largest value at all dissolving times. The morphology of the MSLA after calcination at 500 ℃ had a tubular porous aggregate shape. The crystallinity degree increased with increasing calcination temperature.
3. Quartz was identified in the MSLA at the different calcination temperatures. Another polymorphous crystalline form of silica, cristobalite, only appeared in the 850 ℃ sample, when MSLA was dissolved in an aqueous solution. Muscovite was found in the MSLA residuals due to chemical reactions of OH- and alkali metal. The binding energies of Si 2p and Al 2p shifted after thermal and aqueous solution treatment of the MSLA. In conclusion, the optimum calcination temperature for MSLA used in cementing systems is still tested on the pozzolanic characteristic.

ACKNOWLEDGEMENTS

This work was supported by the Joint Research Fund under a cooperative agreement between the NSFC and Funds for Coal-Based Low-Carbon Technology of Shanxi (No. U1710258); the National Natural Science Foundation of China (Nos. 51574172 and 51804208); Shanxi Province Applied Basic Research Foundation for Youths (No. 201601D021089); the Key Technologies Research and Development Coal-Based Program of Shanxi Province (MQ2014-12); the Research Fund of The State Key Laboratory of Coal Resources and Safe Mining, CUMT(SKLCRSM18KF016); and the China Postdoctoral Science Foundation (2018M632423).

REFERENCES CITED

Biricik, H., AkÖz, F., Berktay, I., and Tulgar, A. N. (1999). “Study of pozzolanic properties of wheat straw ash,” *Cement and Concrete Research*29(5), 637-643. DOI: 10.1016/S0008-8846(98)00249-X

Black, L., Garbev, K., Stemmermann, P., Hallam, K. R., and Allen, G. C. (2003). “Characterisation of crystalline C-S-H phases by X-ray photoelectron spectroscopy,” *Cement and Concrete Research* 33(6), 899-911. DOI: 10.1016/S0008-8846(02)01089-X

Bostrom, D., Skoglund, N., Grimm, A., Boman, C., Ohman, M., Brostrom, M., and Backman, R. (2011). “Ash transformation chemistry during combustion of biomass,” *Energy Fuels*26(1), 85-93. DOI: 10.1021/ef201205b

Callister, W. D., and Rethwisch, D. G. (2010). *Materials Science and Engineering: An Introduction*, Eighth Ed., John Wiley & Sons, New York, New York.

Cociña, E. V., Frías, M., Hernández-Ruiz, J., and Savastano, H. (2013). “Pozzolanic behaviour of a bagasse ash from the boiler of a Cuban sugar factory,” *Advances in Cement Research* 25(3), 136-142. DOI: 10.1680/adcr.11.00066

Cociña, E. V., Savastano, H., Rodier, L., Lefran, M., and Frías, M. (2018). "Pozzolanic characterization of Cuban bamboo leaf ash: Calcining temperature and kinetic parameters," *Waste and Biomass Valorization* 9(4), 691-699.DOI: 10.1007/s12649-016-9741-8

Cociña, E. V., Valencia-Morales, E., González-Rodríguez, R., and Hernández-Ruíz, J. (2003). "Kinetics of the pozzolanic reaction between lime and sugar cane straw ash by electrical conductivity measurement: A kinetic-diffusive model," *Cement and Concrete Research* 33(4), 517-524. DOI: 10.1016/S0008-8846(02)00998-5

Dijkstra, J. J., Van Der Sloot, H. A., and Comans, R. N. (2006). "The leaching of major and trace elements from MSWI bottom ash as a function of pH and time," *Applied Geochemistry* 21(2), 335-351. DOI:10.1016/j.apgeochem.2005.11.003

Dwivedi, V. N., Singh, N. P., Dasa, S. S., and Singh, N. B. (2006). "A new pozzolanic material for cement industry: Bamboo leaf ash," *International Journal of Physical Sciences* 1(3), 106-111.

Fang, X., and Jia, L. (2012). "Experimental study on ash fusion characteristics of biomass," *Bioresource Technology*104, 769-774. DOI: 10.1016/j.biortech.2011.11.055

Fernandes, I. J., Sánchez, F. A. L., Jurado, J. R., Kieling, A. G., Rocha, T. L. A. C., Moraes, C. A. M., and Sousa, V. C. (2017). "Physical, chemical and electric characterization of thermally treated rice husk ash and its potential application as ceramic raw material," *Advanced Powder Technology* 28(4), 1228-1236. DOI: 10.1016/j.apt.2017.02.009

Firdaus, M. Y. N., Osman, H., Metselaar, H. S., and Rozyanty, A. R. (2016). "Preparation and characterization of active SiO_2 from *Cymbopogon citratus* ash calcined at different temperature," *BioResources* 11(1), 2839-2849. DOI: 10.15376/biores.11.1.2839-2849

Font, A., Soriano, L., Moraes, J., Tashima, M. M., Monzó, J., Borrachero, M. V., and Payá, J. (2017). "A 100% waste-based alkali-activated material by using olive-stone biomass ash (OBA) and blast furnace slag (BFS)," *Materials Letters*203, 46-49. DOI: 10.1016/j.matlet.2017.05.129

Frías, M., Savastano, H., Villar, E., De Rojas, M. I. S., and Santos, S. (2012). "Characterization and properties of blended cement matrices containing activated bamboo leaf wastes," *Cement and Concrete Composites*34(9), 1019-1023. DOI: 10.1016/j.cemconcomp.2012.05.005

Gratz, A. J., and Bird, P. (1993). "Quartz dissolution: Negative crystal experiments and a rate law," *Geochimica et Cosmochimica Acta*57(5), 965-976. DOI: 10.1016/0016-7037(93)90033-S

Givi, A. N., Rashid, S. A., Aziz, F. N. A., and Salleh, M. A. M. (2010). "Assessment of the effects of rice husk ash particle size on strength, water permeability and workability of binary blended concrete," *Construction and Building Materials*24(11), 2145-2150. DOI: 10.1016/j.conbuildmat.2010.04.045

Kapur, P. C. (1985). "Production of reactive bio-silica from the combustion of rice husk in a tube-in-basket (TiB) burner," *Powder Technology* 44(1), 63-67. DOI: 10.1016/0032-5910(85)85022-1

Karim, M. R., Hashim, H., and Razak, H. A. (2016). "Assessment of pozzolanic activity of palm oil clinker powder," *Construction and Building Materials*127, 335-343. DOI: 10.1016/j.conbuildmat.2016.10.002

Katare, V. D., and Madurwar, M. V. (2017). "Experimental characterization of sugarcane biomass ash- A review," *Construction and Building Materials* 152, 1-15. DOI: 10.1016/j.conbuildmat.2017.06.142

Li, H. J., Sun, H. H., Tie, X. C., and Xiao, X. J. (2008). "A new method to evaluate the hydraulic activity of Al-Si materials," *Science in China Series E: Technological Sciences* 51(2), 113-120. DOI:10.1007/s11431-007-0064-7

Liu, Z., Tian, D., Hu, J., Shen, F., Long, L., Zhang, Y., Yang, G., Zeng, Y., Zhang, J., and He, J. (2018). "Functionalizing bottom ash from biomass power plant for removing methylene blue from aqueous solution," *Science of The Total Environment* 634, 760-768. DOI: 10.1016/j.scitotenv.2018.04.010

Kljajević, L. M., Nenadović, S. S., Nenadović, M. T., Bundaleski, N. K., Todorović, B. Ž., Pavlović, V. B., and Rakočević, Z. L. (2017). "Structural and chemical properties of thermally treated geopolymer samples," *Ceramics International* 43(9), 6700-6708. DOI: 10.1016/j.ceramint.2017.02.066

Maldonado-Bandala, E. E., Jiménez-Quero, V., and Olguin-Coca, F. J. (2011). "Electrochemical characterization of modified concretes with sugar cane bagasse ash," *International Journal of Electrochemical Science* 6(10), 4915-4926.

Moghal, A. A. B., and Sivapullaiah, P. V. (2012). "Retention characteristics of Cu^{2+}, Pb^{2+}, and Zn^{2+} from aqueous solutions by two types of low lime fly ashes," *Toxicological & Environmental Chemistry* 94(10), 1941-1953. DOI: 10.1080/02772248.2012.732579

Moraes, J., Akasaki, J. L., Melges, J., Monzó, J., Borrachero, M. V., Soriano, L., Payá, J., and Tashima, M. M. (2015). "Assessment of sugar cane straw ash (SCSA) as pozzolanic material in blended Portland cement: Microstructural characterization of pastes and mechanical strength of mortars," *Construction and Building Materials*94, 670-677. DOI: 10.1016/j.conbuildmat.2015.07.108

Morales, E. V., Cociña, E. V., Frías, M., Santos, S. F., and Savastano, Jr., H. (2009). "Effects of calcining conditions on the microstructure of sugar cane waste ashes (SCWA): Influence in the pozzolanic activation," *Cement and Concrete Composites*31(1), 22-28. DOI: 10.1016/j.cemconcomp.2008.10.004

Pagliari, L., Dapiaggi, M., Pavese, A., and Francescon, F. (2013). "A kinetic study of the quartz–cristobalite phase transition," *Journal of the European Ceramic Society* 33(15-16), 3403-3410. DOI: 10.1016/j.jeurceramsoc.2013.06.014

Paparazzo, E., Fanfoni, M., Severini, E., and Priori, S. (1992). "Evidence of Si–OH species at the surface of aged silica," *Journal of Vacuum Science & Technology A: Vacuum Surfaces & Films*10(4), 2892-2896. DOI: 10.1116/1.577726

Rajamma, R., Ball, R. J., Tarelho, L. A., Allen, G. C., Labrincha, J. A., and Ferreira, V. M. (2009). "Characterisation and use of biomass fly ash in cement-based materials," *Journal of Hazardous Materials*172(2-3), 1049-1060. DOI: 10.1016/j.jhazmat.2009.07.109

Roselló, J., Soriano, L., Santamarina, M. P., Akasaki, J. L., Monzó, J., and Payá, J. (2017). "Rice straw ash: A potential pozzolanic supplementary material for cementing systems," *Industrial Crops and Products*103, 39-50. DOI: 10.1016/j.indcrop.2017.03.030

Shen, J., Liu, X., Zhu, S., Zhang, H., and Tan, J. (2011). "Effects of calcination parameters on the silica phase of original and leached rice husk ash," *Materials Letters*65(8), 1179-1183. DOI: 10.1016/j.matlet.2011.01.034

Simonsen, M. E., Sønderby, C., Li, Z., and Søgaard, E. G. (2009b). "XPS and FT-IR investigation of silicate polymers," *Journal of Materials Science* 44(8), 2079-2088. DOI: 10.1007/s10853-009-3270-9

Simonsen, M. E., Sønderby, C., and Søgaard, E. G. (2009a). "Synthesis and characterization of silicate polymers," *Journal of Sol-Gel Science and Technology* 50(3), 372-382. DOI: 10.1007/s10971-009-1907-4

Soltani, N., Bahrami, A., Pech-Canul, M. I., and González, L. A. (2015). "Review on the physicochemical treatments of rice husk for production of advanced materials," *Chemical Engineering Journal* 264, 899-935. DOI: 10.1016/j.cej.2014.11.056

Vassilev, S. V., Baxter, D., Andersen, L. K., and Vassileva, C. G. (2013a). "An overview of the composition and application of biomass ash. Part 1. Phase-mineral and chemical composition and classification," *Fuel* 105, 40-76. DOI: 10.1016/j.fuel.2012.09.041

Vassilev, S. V., Baxter, D., and Vassileva, C. G. (2013b). "An overview of the behaviour of biomass during combustion: Part I. Phase-mineral transformations of organic and inorganic matter," *Fuel* 112, 391-449. DOI: 10.1016/j.fuel.2013.05.043

Wang, Y., Hu, Y., Zhao, X., Wang, S., and Xing, G. (2013). "Comparisons of biochar properties from wood material and crop residues at different temperatures and residence times," *Energy & Fuels* 27(10), 5890-5899. DOI: 10.1021/ef400972z

Xiong, S., Ohman, M., Zhang, Y., and Lestander, T. R. (2010). "Corn stalk ash composition and its melting (slagging) behavior during combustion," *Energy & Fuels*24(9), 4866-4871. DOI: 10.1021/ef1005995

Xu, W., Lo, T. Y., and Memon, S. A. (2012). "Microstructure and reactivity of rich husk ash," *Construction and Building Materials* 29, 541-547. DOI: 10.1016/j.conbuildmat.2011.11.005

Zarina, Y., Al Bakri, A. M., Kamarudin, H., Nizar, I. K., and Rafiza, A. R. (2013). "Review on the various ash from palm oil waste as geopolymer material," *Reviews on Advanced Materials Science* 34(1), 37-43.

Zhang, Z., Han, Z., and Sheng, C. (2016). "Feasibility evaluation of biomass fly ashes from power station using as fertilizer," *Transactions of the Chinese Society of Agricultural Engineering* 32(7), 200-205. DOI: 10.11975/j.issn.10026819.2016.07.028

Zheng, R., Ren, Z., Gao, H., Zhang, A., and Bian, Z. (2018). "Effects of calcination on silica phase transition in diatomite," *Journal of Alloys & Compounds*757, 364-371. DOI: 10.1016/j.jallcom.2018.05.010

Zhu, J., Tang, C., Wei, J., Li, Z., Laipan, M., He, H., Liang, X., Tao, Q., and Cai, L. (2017). "Structural effects on dissolution of silica polymorphs in various solutions," *Inorganica Chimica Acta* 471, 57-65. DOI: 10.1016/j.ica.2017.10.003

Zhu, Y., Hu, J., Yang, W., Zhang, W., Zeng, K., Yang, H., Du, S., and Chen, H. (2018). "Ash fusion characteristics and transformation behaviors during bamboo combustion in comparison with straw and poplar," *Energy & Fuels* 32(4), 5244-5251. DOI: 10.1021/acs.energyfuels.8b00371

Article submitted: September 18, 2018; Peer review completed: October 12, 2018;
Revisions accepted: December 10, 2018; Published: December 12, 2018.
DOI: 10.15376/biores.14.1. 977-995